Biomineralized CdS Quantum Dot Nanocrystals: Optimizing Synthesis Conditions and Improving Functional Properties by Surface Modification

Zhou Yang,[†] Li Lu,[‡] Christopher J. Kiely,[†,‡] Bryan W. Berger,[*,†,§] and Steven McIntosh[*,†]

[†]Department of Chemical and Biomolecular Engineering, [‡]Department of Materials Science and Engineering, and [§]Program in Bioengineering, Lehigh University, Bethlehem, Pennsylvania 18015, United States

[*] Supporting Information

ABSTRACT: An engineered strain of Stenotrophomonas maltophilia (SMCD1) is capable of the direct extracellular biomineralization of CdS quantum dot nanocrystals from buffered aqueous solution of cadmium acetate and L-cysteine without the addition of a chemically reactive precursor. Nanocrystal synthesis is strongly influenced by both the L-cysteine/cadmium acetate ratio and pH of the solution. The observed trends are consistent with L-cysteine acting as both a sulfur source and nanocrystal capping agent. Enzymatic turnover of L-cysteine by a putative cystathionine γ-lyase forms reactive sulfur in solution, removing the requirement for addition of reactive sodium sulfide typical of most other biomineralization approaches. The utility of the biomineralized quantum dots is demonstrated by phase transfer from the aqueous to the organic phase and subsequent incorporation into a quantum dot sensitized solar cell and chemical growth of a ZnS shell onto the biomineralized CdS core.

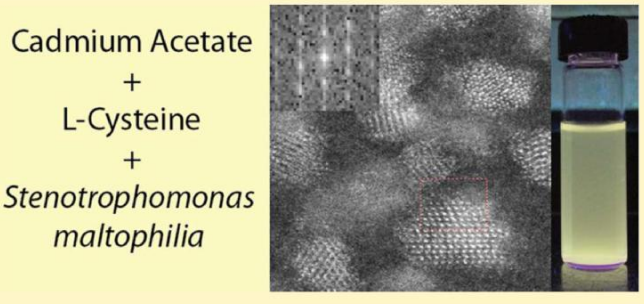

1. INTRODUCTION

Biomineralization, and related bioinspired synthesis, utilizes engineered biological systems and molecules to drive and direct the synthesis of inorganic materials.[1−4] Natural systems, from mollusk shells[5−8] to sea sponges, [9 −13] have evolved to both mineralize and structure materials, often over multiple length scales. This has served as inspiration for studies that seek both fundamental understanding of the biological processes, and new approaches to controlled synthesis. While these natural materials typically serve a structural role, there is great interest in engineering biological systems to create functional materials. Biomineralization offers a route to low temperature, aqueous phase synthesis of crystalline materials, perhaps in structures or morphologies that may not be accessible through purely chemical routes. This intrinsically greener synthesis route has the potential to reduce production cost and lead to materials with new or improved functionality.

In this work we focus our attention toward producing cadmium sulfide quantum dot nanocrystals (QDs) by biomineralization. CdS QDs have potential applications in a number of devices, including display technologies, in vivo or in vitro biomedical imaging/detection and quantum-dot solar cells.[14−18] Commonly utilized chemical procedures, such as hot-injection methods, need multiple organic solvents, expensive precursors, and high reaction temperatures.[19]

A number of groups have demonstrated the potential of engineered or natural biomolecules or biological systems as structure directing agents during the chemical synthesis of nanocrystalline CdS.[20−24] In these cases, a reactive sulfur source, typically sodium sulfide, is added to a cadmium containing solution. In the absence of the biological component to template nanocrystal structure, this mixture would yield a bulk material. For example, Sweeney et al. achieved intracellular CdS nanocrystal synthesis within E. coli upon addition of reactive sodium sulfide to a solution of the bacteria and cadmium chloride.[22] In this case, the bacterial system served to direct the formation of CdS nanocrystals. Flynn et al. utilized the same reactants in the presence of engineered peptide-phage constructs to direct the nucleation and growth of CdS nanocrystals.[25] A similar viral assembly approach has been utilized to achieve control over orientation during crystal growth to yield nanowire morpholgies.[24]

Intriguingly, a small number of prior reports indicate CdS nanocrystal formation without the addition of a reactive sulfur compound. The seminal work of Dameron et al. demonstrated CdS nanocrystal growth within Candida glabrata and Schizosaccharomyces pombe.[26] They suggested a mechanism of cadmium ion sequestration within peptide complexes and subsequent biomineralization utilizing sulfide ions generated from an upregulated cellular process. They reported the formation of CdS QDs having a relatively tight particle size distribution, i.e., 2.9 ± 0.5 nm. A number of other reports similarly do not explicitly add an additional sulfur source to

achieve CdS mineralization,[27−29] with some indicating that the amino acid cysteine may act as the sulfur source upon conversion via a cysteine desulfhydrase.[27,29,30] Where nanocrystals are formed, the biological system is both generating a reactive sulfur species and influencing nanocrystal growth.

In a recent development, we reported an engineered strain of the bacteria Stenotrophomonas maltophilia (SMCD1) capable of promoting extracellular CdS nanocrystal formation in the quantum confined size range in a highly reproducbile manner.[31−33] Nanocrystal mineralization was realized through the addition of significant concentration of the amino acid L-cysteine, that acts as a sulfur source and capping agent.[34−39] No CdS QDs were formed without the addition of L-cysteine. These biomineralized nanocrystals also have a tight size distribution, for example, 2.75 ± 0.68 nm, as well as the added advantage that the mean particle size, and resulting optical properties, that may be deliberately controlled via the incubation time. In further work we directly linked this extracellular synthesis to the expression of a putative cystathionine γ-lyase capable of both catalyzing mineralization and templating nanocrystal growth.[32] This class of enyzmes catalyzes the formation of pyruvate, ammonia, and hydrogen sulfide from L-cysteine.[40] The particular cystathionine γ-lyase produced by SMCD1 provides the critical combination of mineralization catalysis, through the formation of reactive H_2S, and intrinsic nanocrystal templating required to control QD biomineralization.[32]

Herein the sensitivity of Stenotrophomonas maltophilia SMCD1-mediated CdS biomineralzaion to reactant concentration and pH is systematically investigated to provide further insight into the QD formation mechanism. Additionally, the outstanding question as to whether or not these biomineralized CdS nanocrystals can be utilized for optical applications is specifically addressed. A facile route for aqueous to organic phase transfer of the biosynthesized CdS nanocrystals is demonstrated which further broadens their scope for practical utilization as functional nanomaterials. The now organic soluble biomineralizated CdS nanocrystals are integrated into a functioning quantum dot sensitized solar cell and also utilized in a chemical synthesis procedure to generate CdS/ZnS core−shell nanocrystals.

2. EXPERIMENTAL SECTION

Bacteria for our experiments were isolated from soil on the mountaintop campus of Lehigh University, Bethlehem, PA, U.S.A. The bacterial isolate was evolved through iterative selection for cadmium resistance during growth on Luria−Bertani broth agar plates in the presence of increasing concentrations of cadmium acetate. A specific strain, denoted hereafter as SMCD1, was isolated and identified through 16S rDNA genotyping to confirm that it was Stenotrophomonas maltophilia.[31]

SMCD1 cells for the following experiments were grown in Lysogeny broth (Alfa Aesar) for 12 h at 37 °C. CdS QDs synthesized by SMCD1 cells were centrifuged and resuspended (optical density (OD) at 600 nm of 0.5) in tris-(hydroxymethyl)aminomethane-HCl (Tris HCl: 99%, Alfa Aesar; Tris base: ultrapure grade, Amresco) buffer at pH 9.0 unless otherwise noted. This optical density was chosen as it represents logarithmic growth phase of S. maltophilia in culture. Cadmium acetate (99.999%, Alfa Aesar) and L-cysteine (98%, Alfa Aesar) were added in controlled concentrations prior to incubation with shaking at 37 °C for prescribed times. The cell mass was separated from the CdS nanocrystals by centrifugation at 5000 rpm, followed by syringe filtration (0.2 μm) of the supernatant. The aqueous phase QD solutions thus obtained are referred to as harvested solutions. Such solutions were dialyzed (Snakeskin 3500 MWCO; Thermo Pierce) against ultrapure water to remove residual cadmium acetate, L-cysteine, and the buffer salts. The residual concentration of free thiol after these steps was found to vary between 0.2 and 0.5 mM as measured using Ellman's reagent.[41] These are referred to as purified aqueous solutions. Post pH adjustment of the purified aqueous solution was carried out by adding either acetic acid (99.7%, Alfa Aesar) or tetramethylammonium hydroxide (98%, Alfa Aesar).

The biosynthesized aqueous soluble CdS QDs could be transferred into 1-octodecene (ODE, 90%, Alfa Aesar) in the presence of oleylamine (98%, sigma Aldrich) capping agent. In a typical phase transfer experiment, 15 mL of the purified aqueous CdS QD sample was shaken with 5 mL of oleylamine and 10 mL of ODE. The solution was degassed for 10 min and then stirred vigorously under argon for 1 h at 60 °C. A centrifuge (5000 rpm)/decantation procedure was applied for separation of the organic and aqueous phases. A hexane and methanol (volume ratio of 1:3) solution was contacted with the organic phase as an extraction solvent to purify the organic phase; this process was repeated three times.

Ligand capping exchange from oleylamine to oleic acid (90%, Alfa Aesar) was accomplished through addition of oleic acid to the purified oleylamine capped CdS QDs. Typically, 20 mL of the oleylamine capped CdS QDs in ODE was mixed with 10 mL oleic acid. The solution was degassed for 10 min and placed under argon for 3 h at room temperature. The same hexane/ methanol extraction procedure as previously described was utilized prior to precipitation of the QDs by methanol addition. The isolated precipitate is readily soluble in chloroform to yield an optically clear solution.

Growth of a ZnS shell on CdS QDs was carried out following the procedure described by Chen et al.[42] using oleic acid capped CdS QDs as the core material. A 2 mL quantity of CdS QDs in chloroform was mixed with 10 mL of ODE. The solution was degassed in argon for 30 min and then heated to 50 °C prior to dropwise addition of 0.5 mL of 0.01 M zinc diethyldithiocarbamate ($Zn(DDTC)_2$, > 99%, TCI America) under argon flow. The solution was then immediately heated to 170 °C. After 20 min, the solution was cooled to 120 °C and a second injection of $Zn(DDTC)_2$ carried out before once again heating to 170 °C. This procedure was repeated for a third time. Finally, the temperature of the solution was increased to 240 °C and maintained for 20 min. The final solution was washed and purified by the same hexane/methanol extraction procedure. The CdS/ZnS QDs so generated were precipitated by acetone addition and then resuspended in chloroform.

UV−vis absorption spectra (UV-2600, Shimadzu) and photoluminescent emission spectra (QuantaMaster 400, Photon Technology International) from the various colloids were collected. Coumarin 1 (Sigma-Aldrich) in ethanol was used as a standard for quantum yield determination. Samples for high angle annular dark field scanning transmission electron microscopy (HAADF-STEM) imaging and X-ray energy dispersive spectroscopy (XEDS) analysis were prepared by drop casting QD suspensions onto holey carbon-coated copper TEM grids. The samples were analyzed in a 200 kV aberration corrected JEOL ARM 200CF analytical electron microscope equipped with a Centurio XEDS system.

QD sensitized solar cells were fabricated using commercially available glass slides coated with F-doped tin oxide (FTO, ~7 Ω/sq, Sigma-Aldrich) that were covered with a TiO_2 blocking layer by dipping it into a 40 mM $TiCl_4$ (>99.0%, Sigma-Aldrich) solution, followed by sintering in air at 500 °C for 3 h. A second mesoporous TiO_2 film (TiO_2 paste, 27.0 wt %, Sigma-Aldrich) was deposited on top of the blocking layer with a doctor blade followed by sintering at 500 °C for 1 h in air. The CdS QDs capped by oleic acid in chloroform were loaded into the mesoporous TiO_2 by drop casting. The completed photoelectrode was dried under ambient conditions. The counter electrode was prepared by painting a conductive gold paste (Electron Microscopy Sciences) onto FTO glass. The working and counter electrodes were assembled into a sandwichstructure. The electrolyte was prepared by dissolving 0.5 M Na_2S (98%, Alfa Aesar), 0.5 M S (99.5%, Alfa Aesar) and 0.055 M NaOH (99.99%, Alfa Aesar) in water. The photocurrent density−voltage (J-V) performance characteristic was measured using an electrochemical workstation (Reference 600, Gamry Instruments) under irradiation (AM 1.5 G solar simulator, model no. 10500, ABET Technologies) with an incident light intensity of 100 mW cm^{-2}.

3. RESULTS AND DISCUSSION

3.1. Influence of Synthesis Conditions on Nanocrystal Growth. Strain SMCD1 is capable of biomineralization of CdS nanocrystal quantum dots utilizing cadmium acetate as the cadmium source and L-cysteine as the sulfur source and capping agent.[31] We have previously demonstrated that the average biomineralized CdS nanocrystal size increases with increasing incubation time. The hypothesized mechanism is that the bacteria produce a cystathionine γ-lyase capable of converting the L-cysteine thiol group into reactive H_2S. Such an enzyme has been identified associated with the biomineralized CdS nanocrystals.[31] In order to further understand the relationship between growth conditions and nanocrystallite size, we investigated the influence of L-cysteine/cadmium acetate ratio with variable cadmium acetate concentration between 0.25 and 4 mM with constant L-cysteine (8 mM) and cell (OD_{600} = 0.5) concentration, and constant buffer pH of 9.0. This yields a theoretical range of S:Cd ratios from 32:1 to 2:1. The absorbance and emission spectra of the harvested aqueous solutions after 30 min incubation at 37 °C are shown in Figure 1.

The first excitonic absorption peaks, Figure 1a, shift to longer wavelength with increasing S:Cd ratio. No absorbance peak is observed at a S:Cd ratio of 2:1 as the peak is obscured by the absorbance of the buffer solution below 300 nm. The corresponding emission peak positions, Figure 1b, shows the same red-shift trend with increasing S:Cd ratio, consistent with the change in visible photoluminescence under UV light, inset in Figure 1b. The absorbance spectra as a function of incubation time were also collected at S:Cd ratios of 32:1 and 8:1. The absorption peak wavelength systematically increases as a function of incubation time in both cases, Figure 1c; however, the peak intensity is significantly greater at decreased S:Cd ratio. The optical properties reported here are all within the quantum confinement range for CdS, indicating the formation of CdS nanocrystals[31] (Figure S1). The band gap of bulk CdS is known to be 2.5 eV (496 nm).[43] The observed red-shift in our samples is attributable to an increase in the average size of the quantum dots as the S:Cd increases, suggesting that the enzymatic production of H_2S may be the limiting factor in particle growth. For reference, our previous work[31] experimentally demonstrated by correlation of optical and electron microscopy data that adsorption peak maxima of 324, 344, and 368 nm, correspond to biomineralized nano-crystallite sizes of 2.75 ± 0.68, 3.04 ± 0.75, and 3.36 ± 0.95 nm, respectively.

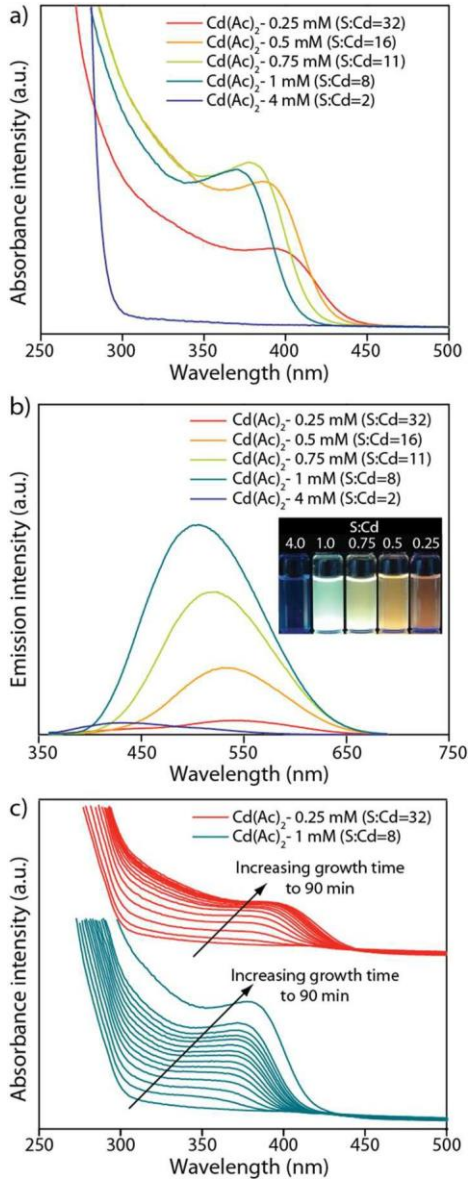

Figure 1. Aqueous phase optical properties of harvested CdS nanocrystal solutions grown with different concentrations of cadmium acetate ($Cd(Ac)_2$) ranging from 0.25 to 4 mM. (a) UV−vis absorption spectra. (b) Fluorescence emission spectra using a 350 nm excitation wavelength. Inset is a photograph of the cultures illuminated under UV light showing the evolution of fluorescent color. (c) Temporal evolution of absorbance spectra using 0.25 mM and 4 mM concentrations of $Cd(Ac)_2$. Each line is separated by a 4 min incubation time interval up until 50 min, and after that the spectra were sampled at 60 and 90 min.

L-Cysteine acts as both the sulfur source and capping agent during nanocrystal biomineralization.[31] The optimization of growth conditions is thus dependent on the interplay of factors influencing this dual role. First, the concentration of L-cysteine will influence reactant and capping agent availability. Second, solution pH will influence both the protonation/deprotonation

of the thiol group on L-cysteine (pK_a = 8.3[44]) and the potential formation of the dimer, cystine, which can quench the fluorescence.[35,45] Cystine formation is favored at elevated pH. In order to elucidate and deconvolute these multiple overlapping parameters, the influence of L-cysteine concentration (Figure 2) and pH during synthesis (Figure 3), as well as the pH of the QD solution after synthesis (Figure 4), was studied.

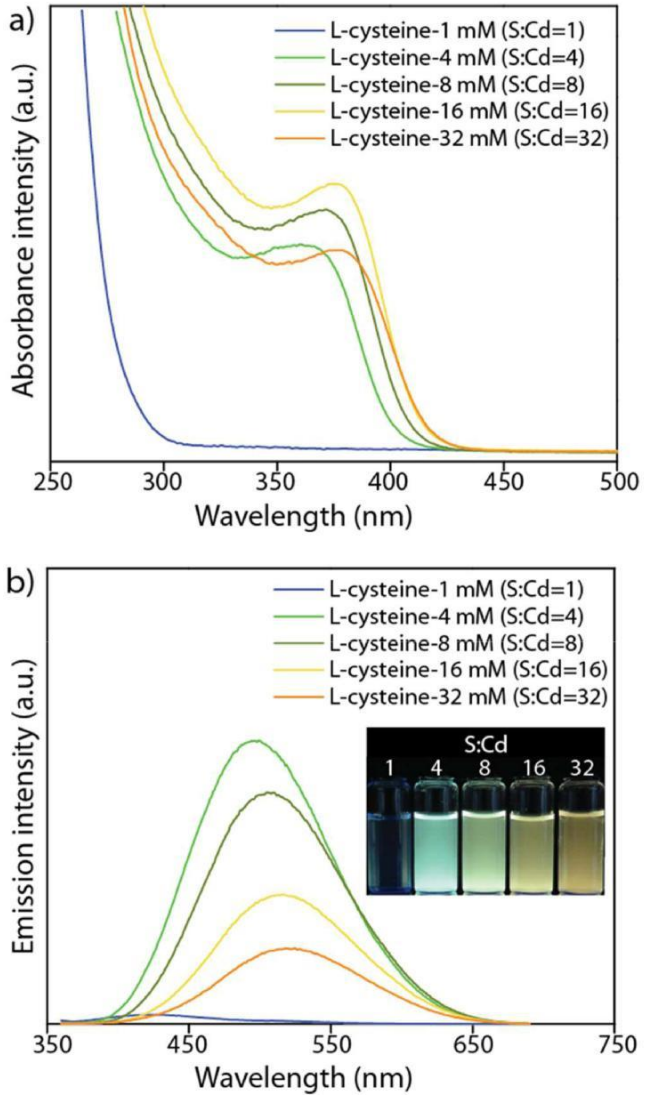

Figure 2. Aqueous phase optical properties of CdS QDs harvested after 30 min incubation time with varying initial concentration of L-cysteine varying between 1 and 32 mM. (a) UV−vis absorption spectra of the as-grown cultures; (b) fluorescence emission spectra using a 350 nm excitation wavelength. Inset is a photograph of the visible fluorescence from these cultures under UV illumination.

Figure 2 shows absorption and photoluminescence proper-ties respectively of CdS nanocrystals grown as a function S:Cd ratio induced by varying the L-cysteine concentration, from 1 to 32 mM, at constant cadmium acetate (1 mM) and cell (OD_{600} = 0.5) concentration and a pH of 9.0. The absorbance spectra (Figure 2a) show well-defined peaks with maxima showing a red-shift trend with increasing S:Cd ratio, corresponding to increasing L-cysteine concentration. As with the lowest S:Cd ratio in Figure 1a, the absorption peak for S:Cd ratio in Figure 2a is obscured by the absorption of the buffer solution.

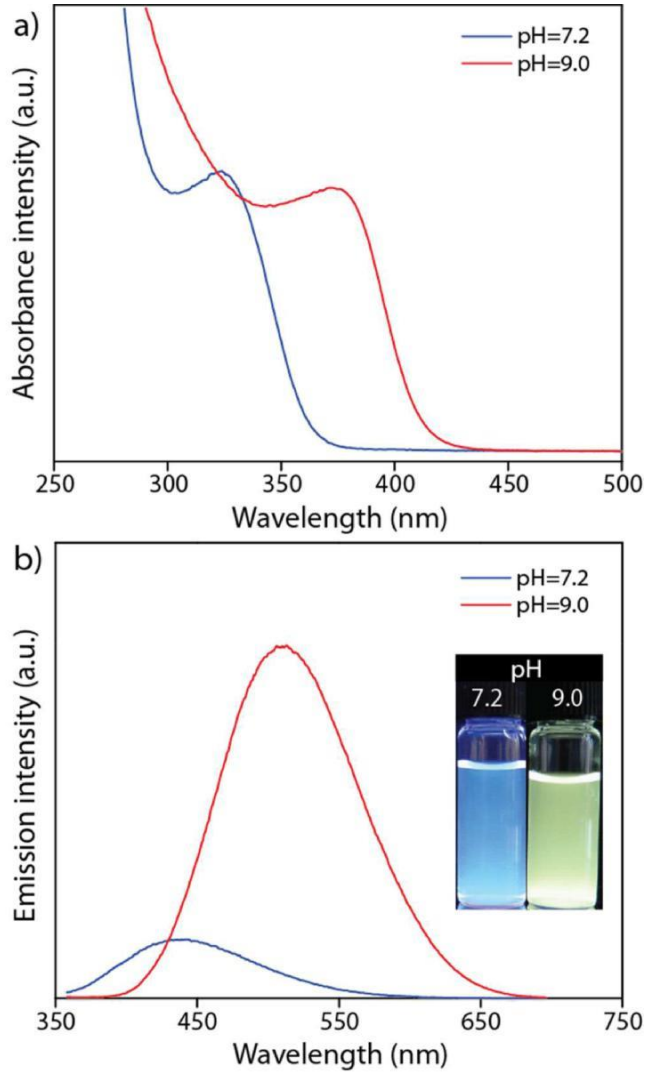

Figure 3. Optical properties of harvested CdS nanocrystal solutions after 30 min incubation time with varying initial pH adjusted by changing the Tris-HCl buffer ratios. (a) UV−vis absorption spectra; (b) Fluorescence emission spectra using a 350 nm excitation wavelength. Inset is a photograph of the visible fluorescence from the cultures when illuminated under UV light.

Switching the buffer to M9 minimal media reveals a peak at 308 nm, Figure S2. The emission spectra (Figure 2b) show the same systematic trend with the peak maxima wavelength progressively red-shifting with increasing L-cysteine concen-tration, consistent with the visible photoluminescence observed under UV light.

The CdS nanocrystal growth rate is clearly sensitive to the S:Cd ratio, with values between 4:1 and 16:1 yielding stable nanocrystal solutions after 30 min of incubation that show optical properties consistent with CdS particles in the quantum confined size range. At higher S:Cd ratios, the particle solutions are unstable, likely due to an increase in particle size and the relatively poor solution stabilization provided by L-cysteine. Figures 1 and 2 also reveal practical limitations in both the upper Cd concentration and lower limit of L-cysteine concentration. A Cd concentration of 4 mM leads to minimal nanocrystal growth, most likely due to the toxicity of Cd to the cell.[46] The original directed evolution approach selected a viable bacterial strain at 1 mM Cd. An L-cysteine concentration

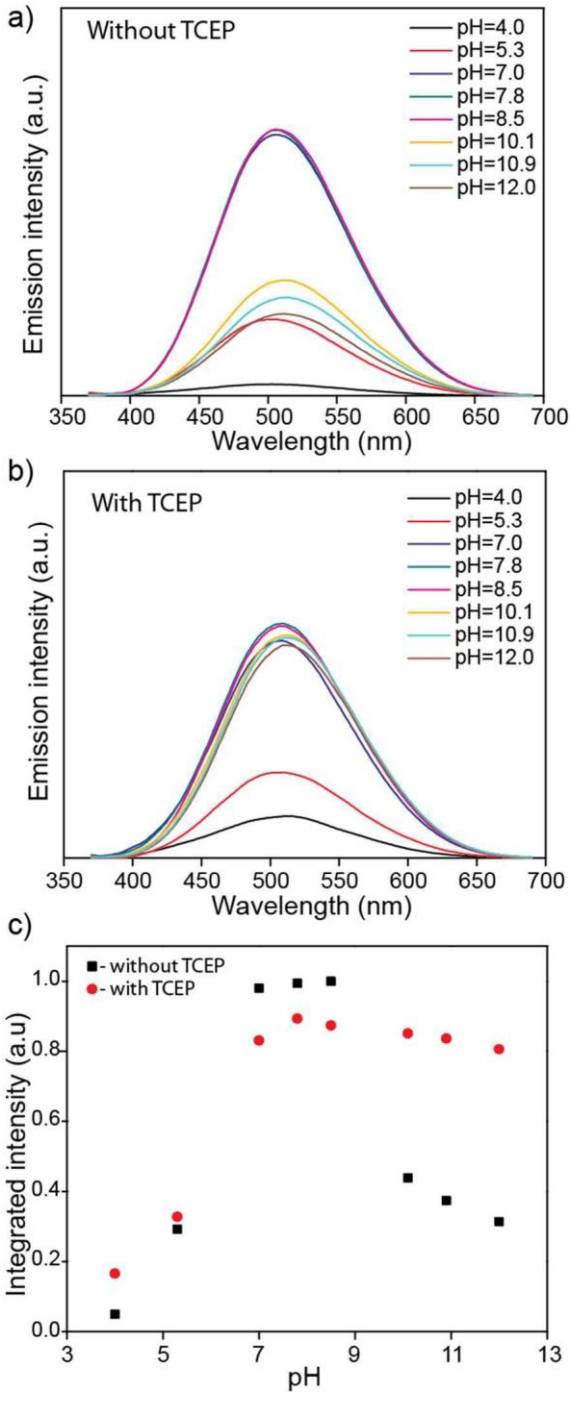

Figure 4. Aqueous phase optical properties of purified CdS nanocrystal solutions after 30 min incubation time with varying pH of the purified solution. (a) UV−vis absorption spectra of the as-grown cultures; (b) fluorescence emission spectra using a 350 nm excitation wavelength; (c) normalized integrated photoluminescence intensity.

below 4 mM also leads to minimal nanocrystal growth, which in this case is due to a combination of low availability of reactive sulfur and utilization of the amino acid in unrelated cellular processes.

Within the range of stable solutions, increasing the S:Cd ratio leads to a red-shift of optical properties, consistent with an increase in nanocrystallite size and consistent with other reports of varying S:Cd ratio during chemical synthesis with reactive chemical precursors added to solution.[47,48] Wang et al.[48] proposed that at low cysteine/Cd ratio, the Cd precursor is primarily in the form of reactive Cd-cysteine monothiol-complexes that initiate large population of nuclei, and consequently a larger number of smaller particles are formed during synthesis. In contrast, at higher cysteine/Cd ratio, they suggest that the Cd precursor is mainly in the form of a lower reactivity dithiol-complex, leading to a smaller number of nuclei and subsequent increased average size of QD. Critically Wang et al. also discuss that increased cysteine concentration also favors the formation of the cystine dimer. The potential formation of this dimer is likely of increased importance to our biomineralization process as cysteine acts as both capping agent and sulfur precursor. No reactive chemical precursor such as Na_2S is added for biomineralization, instead strain SMCD1 produces the putative cystathionine γ-lyase enzyme previously identified as responsible for mineralization and templating.[32] This class of enzyme converts L-cysteine or L-cystine to H_2S, pyruvic acid, and NH_3,[49] thereby providing the reactive sulfur required for solution phase CdS biomineralization. It may be that the presence of the dimer reduces the number of initial nuclei through slower enzymatic turnover.

Figure 3 shows the influence of buffer pH during growth on the optical properties of the nanocrystals at a fixed initial concentration of cadmium acetate (1 mM), L-cysteine (8 mM), and cells (OD_{600} = 0.5). Figure 3a shows that the nanocrystal absorbance peak wavelength of 372 nm at a growth pH of 9.0, is red-shifted by 51 nm when compared to that obtained from a synthesis carried out at pH 7.2. The corresponding emission peak wavelengths (Figure 3b) are similarly red-shifted, i.e., 512 and 440 nm at growth pH 9.0 and 7.2, respectively. The corresponding quantum yields of these harvested particles are 0.7 and 1.9%, for the pH 7.2 and 9.0 solutions, respectively. The reported optimal activity of cystathionine γ-lyase enzymes is above pH 8.0[50−52] which is in agreement with the observed red-shift upon increasing pH in our experiments and further supporting the concept of the growth rate being dependent on the availability of reactive sulfur formed by the enzyme.

Figure 4 shows the photoluminescence intensity of various purified aqueous QD samples as a function of solution pH adjusted after synthesis. The synthesis was carried out at a pH of 9.0. The corresponding absorbance spectra peak maxima wavelength and intensity are unaffected by changing the pH after synthesis (Figure S3). The pH was adjusted with acetic acid or tetramethylammonium hydroxide. The optimal (maximum) photoluminescence intensity was obtained by adjusting the pH after synthesis to between 7.0 and 8.5, which is consistent with the pK_a of the thiol group in L-cysteine being 8.3. The corresponding quantum yield in this pH range was determined to be 2.3%. The increased quantum yield of the post-treated sample when compared to the as-harvested solution is most likely due to the purification of the aqueous phase via dialysis. Decreasing the pH even further to 4.0 leads to a significant decrease in photoluminescence intensity and a corresponding decrease in quantum yield to 0.1%. This degradation is in-line with previous reports, where a pH value significantly below the pK_a of the thiol group in the QD capping agent leads to suppression of the photoluminescence[36,53] in the absence of any specific cadmium-capping agent complex formation.[54]

The photoluminescence intensity similarly decreases upon increasing the pH above 8.5 and the quantum yield drops to 0.7% at pH 12. This is probably due to the dimerization of L-cysteine to cystine which has been previously reported to

quench photoluminescence.[45] Cystine can be reduced upon the addition of tris(2-carboxyethyl)phosphine hydrochloride (TCEP)[45] to the elevated pH solution, leading to an increase in photoluminescence (Figure 4b,c). All of this data clearly demonstrates the role of L-cysteine as a capping agent in our biomineralized CdS QD system. This is in addition to its role as a sulfur source for the likely enzymatic turnover of L-cysteine to form H_2S.

The quantum yield of these biomineralized CdS QDs is broadly comparable to the majority of other reports on aqueous phase chemically synthesized CdS solutions[55,56] although occasionally quantum yields up to 15% have been obtained.[57,58] In aqueous solution, the quantum yield may be limited by the relatively poor capping of L-cysteine; indeed, L-cysteine has been reported to quench the photoluminescence of aqueous CdS QDs.[59] Certainly a value of around 2.3% when capped with L-cysteine in the aqueous phase appears to be the maximum achievable quantum yield through the current cell-based biomineralization route.

3.2. Phase Transfer and Biomineralized Nanocrystal Utilization. In order to expand the application space for biomineralized QDs, a facile method (as detailed in the Experimental Section above) was developed to transfer the L-cysteine capped CdS QDs from the aqueous phase to oleylamine capped QDs in 1-octadecene. The absorbance and photoluminescence emission spectra of the QDs in the aqueous phase and in the organic phase after phase transfer are shown in Figure 5a,b, respectively. The efficiency of the phase transfer procedure is indicated by the low level of photoemission observed under UV illumination for the (lower) aqueous phase after transfer, and correspondingly high level of photoemission from the (upper) organic phase, inset in Figure 5a. The maxima of the absorbance and photoemission peaks both red-shift, by 15 and 5 nm, respectively, upon transfer to the organic phase due to the change of capping agent. The quantum yield of the CdS QDs in the organic phase increases to 2.9% from an initial value of 1.5% in the aqueous phase, most likely due to more efficient QD capping in the organic phase. The lower initial quantum yield in the aqueous phase when compared to the QDs in Figure 5 is due to the smaller size of the nanocrystals.[31] This demonstrated facile procedure for aqueous to organic phase transfer enables integration of the biomineralized QDs into more standard processing procedures.

First, we demonstrate that the phase transferred biominer-alized CdS quantum dots can be utilized in a quantum dot sensitized photovoltaic cell by drop casting the solution into a TiO_2 electrode, Figure 6. Addition of the biomineralized CdS QDs leads to both increased open circuit voltage, V_{OC}, from 0.32 to 0.60 V, and increased short circuit current density, J, from 0.41 to 0.55 mA/cm^2. In addition, there is an increase in fill factor from 41% to 50%, which translates to a corresponding increase in device efficiency to 0.17%. These performance improvements upon integration of biomineralized CdS quantum dot nanocrystals into the solar cell are in line with prior reports utilizing chemically synthesized materials.[60−62] It should be noted that these basic photovoltaic cells are not fully optimized and here only serve to illustrate the potential for technological use of these biomineralized CdS QD materials.

To further demonstrate the possible utility of these biomineralized QDs, CdS/ZnS QDs were synthesized from the phase transferred CdS by following a single precursor method previously developed by Chen et al.[42] The absorbance and emission spectra of the QDs before and after ZnS shell

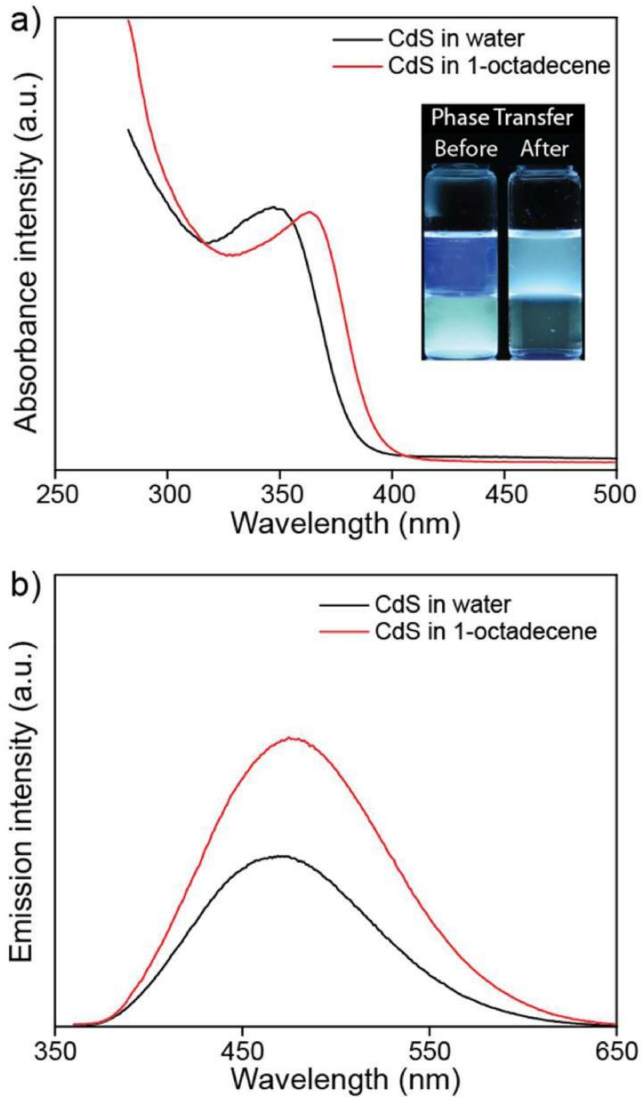

Figure 5. Optical properties of CdS QDs in aqueous phase and 1-octadecene after phase transfer. (a) UV−vis absorption spectra; (b) fluorescence emission spectra using a 350 nm excitation wavelength. Inset in (a) is a photograph of the biphase solution illuminated under UV light before and after transfer.

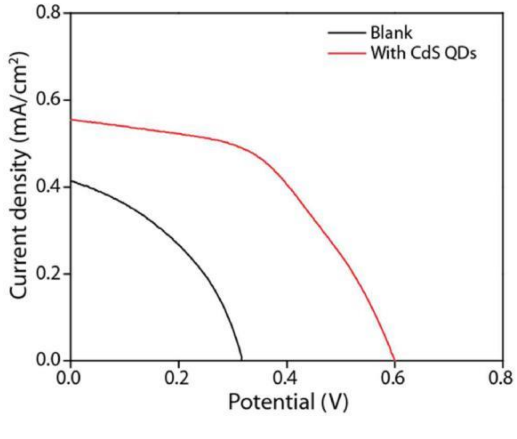

Figure 6. Current−voltage characteristics of the CdS quantum dot based cells measured under 1 sun illumination (AM 1.5 G, 100 mW/cm^2). $V_{Open\ Circuit}$ = 0.60 V, $J_{Short\ Circuit}$ = 0.55 mA/cm^2, fill factor = 50%, efficiency = 0.17%.

growth are shown in Figure 7. While the emission spectrum of the CdS core material shows a broad trap-state emission with a large Stokes shift of 135 nm, the CdS/ZnS QDs exhibit a dominant band-edge emission with a Stokes shift of 20 nm. This indicates that the growth of a ZnS shell on the biomineralized QDs eliminates the majority of the surface traps and is consistent with previous reports for chemically synthesized materials.[42,63−65] The ZnS growth procedure requires capping agent exchange on the seed QD to oleic acid which causes an accompanying quenching of CdS photoluminescence, as compared to the original oleylamine capped CdS QDs. The quantum yield of oleic acid capped biomineralized CdS QDs prior to ZnS growth is only 0.8%, but increases to 2.7% after ZnS shell growth, suggesting effective passivation of CdS surface trap states.

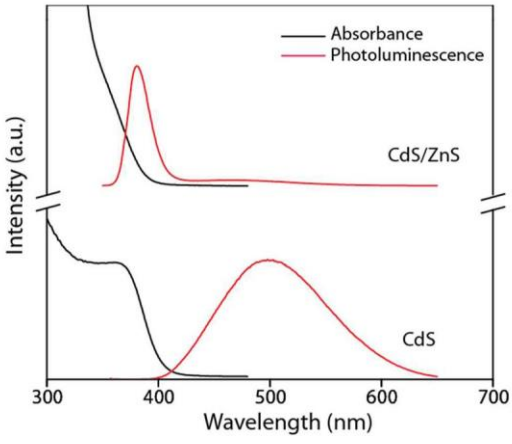

Figure 7. Normalized optical characteristics of the core CdS QDs capped with oleic acid and resultant core−shell CdS/ZnS QDs. Black lines are UV−vis absorption spectra; red lines are fluorescence emission spectra using a 350 nm excitation wavelength.

High angle annular dark field scanning transmission electron microscopy (HAADF-STEM) was utilized to visualize the size and crystalline nature of the CdS and CdS/ZnS QDs, and complementary X-ray energy dispersive spectroscopy (XEDS) analysis was performed to confirm the coexistence of Cd and Zn within individual core−shell QDs. Well dispersed CdS QDs prior to ZnS growth are observable in Figure 8a. Corresponding higher resolution images are able to resolve atomic structure within individual particles (Figure 8b). Fitting of lattice fringe spacings and intersections angles (Figure S4) indicate that the biomineralized CDs QDs are in fact a mixture of the hexagonal wurtzite and cubic zinc-blende phases.[31] Comparable particle dispersion, crystal quality, and polymorph distribution are observed for the CdS/ZnS QDs, as shown in Figures 8e,f and S4, respectively. XEDS analysis from individual QDs confirmed that the as-synthesized CdS particles contain only Cd and S (Figure 8d) while the XEDS spectrum of a single CdS/ZnS particle confirms the presence of Cd, Zn, and S (Figure 8h). A small Si-escape peak from the detector material is present in the XEDS spectra; the copper peaks arise from the TEM support grid. Although there is not enough contrast to directly observe a distinct core−shell structure in these images, the thickness of the ZnS layer can be estimated by comparison of the particle size distributions acquired before and after ZnS shell deposition as measured from analysis of at least 200 particles per sample. The mean particle size of the CdS only QDs is 4.28 ± 0.68 nm with a dispersion of 16% (Figure 8c). After ZnS growth, the mean size increases to 4.79 ± 0.73 nm with a dispersion of 15% (Figure 8g). This is consistent with the deposition of about a monolayer of ZnS on the exterior surface of a CdS core.[65]

The formation of a chemically synthesized ZnS shell on the biomineralized CdS core is clearly demonstrated by the change in mean particle diameter, XEDS analysis from individual particles and a shift from trapped state to band edge emission after the ZnS shell growth procedure. All of these combined observations are in agreement with prior reports of ZnS shell growth on CdS.[65] Direct imaging of a ZnS shell was not feasible but the measured diameter increase indicates a single ZnS layer has been deposited.

While the quantum yield increases upon phase transfer to the organic phase with oleylamine capping, it decreases again upon

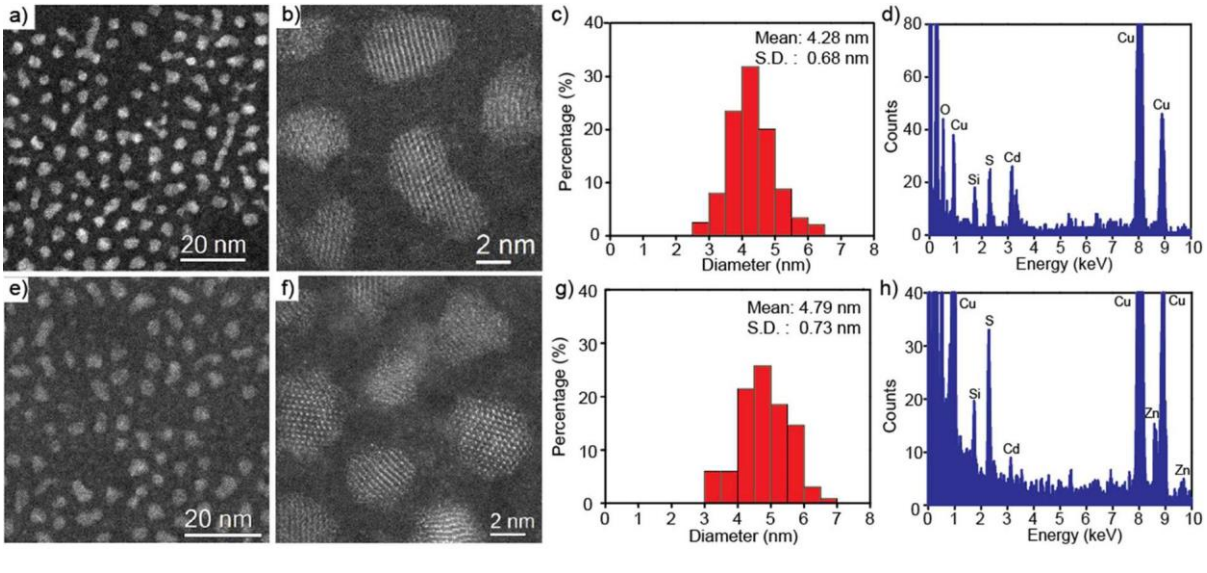

Figure 8. (a and b) HAADF-STEM images of the CdS QDs; (c) particle size distribution of the CdS QDs; (d) XEDS analysis from an individual CdS QD. (e and f) HAADF-STEM images of the CdS/ZnS QDs. (g) Particle size distribution of the CdS/ZnS QDs. (h) XEDS analysis of the CdS/ZnS QDs. A small Si-escape peak from the detector material is present in the XEDS spectra; the copper peaks arise from the TEM support grid.

capping with oleic acid. Growth of ZnS again increases the quantum yield. The biomineralized QDs are crystalline, and the surface traps are significantly decreased upon ZnS shell growth; however, the maximum quantum yield achieved in all conditions is below three percent. Improvement in QY is hence a fertile area for further work in these biomineralized systems.

While the solar cell performance results and ZnS shell growth are in good general agreement with previous reports utilizing CdS and CdS/ZnS core−shell QDs, what is remarkable about this study is that an optimized biomineraliza-tion procedure can produce crystalline CdS QDs of sufficiently high enough quality that they can be utilized in a similar manner to chemically synthesized materials. While clearly there is still some way to go in optimizing the biomineralization procedure to produce the highest quality QDs in terms of absolute quantum yield, the potential cost benefits over chemical synthesis routes are considerable. The biomineralized materials are fabricated at 37 °C in water in an open laboratory container from low-cost cadmium acetate and L-cysteine. This synthesis stands in stark contrast to typical chemical synthesis routes that must be conducted at elevated temperature, often at temperatures exceeding 250 °C, in organic solvent under inert atmosphere or vacuum under strictly dry conditions. These latter conditions are typically required due to the reactivity of the precursor materials. There may well be an application space where the lower QY may be outweighed by the potential environmental and cost benefits of biomineralization. Work is ongoing to both further improve the QY of our CdS particles and also to expand the palette of optoelectronic materials that can be made by such biomineralization routes.

4. CONCLUSIONS

We have presented a detailed study of the biosynthesized CdS QDs from Stenotrophomonas maltophilia (SMCD1). The growth parameters, such as the concentrations of cadmium acetate and L-cysteine, and the pH of the buffer, have been systematically investigated. We have identified the most appropriate cadmium acetate, L-cysteine and basic buffer concentrations, and pH conditions that are required for successful CdS QDs growth. The optical properties can be controlled and tuned by varying the growth conditions, especially the growth time. In addition, we have demonstrated that the biosynthesized water-soluble CdS QDs can be efficiently transferred to organic solvents with a concurrent improvement in their optical properties. Furthermore, CdS/ ZnS quantum dots with core−shell morphologies have also been successfully generated which display suppression of CdS surface trap states. By utilizing such postgrowth treatments on the as-grown cell-derived CdS particles (i.e., solvent exchange, stabilizing ligand exchange, and ZnS shell formation), QD materials have been produced which show comparable properties to their chemically synthesized CdS QD counter-parts. This work provides a better understanding of the production of CdS QDs by cell based methods and demonstrates their potential for future technological applica-tion.

ASSOCIATED CONTENT

* Supporting Information

TEM images of single CdS nanocrystals and correspond-ing fast Fourier transforms and their lattice fitting data; optical properties of aqueous CdS in M9 media buffer with different concentration of L-cysteine; absorbance spectra of CdS QDs solutions at different pH with and without TCEP; TEM images of single core/shell CdS/ ZnS nanocrystals and corresponding fast Fourier trans-forms and their lattice fitting data. (PDF)

AUTHOR INFORMATION

Corresponding Authors

* E-mail: berger@lehigh.edu.

* E-mail: mcintosh@lehigh.edu.

Author Contributions

These authors contributed equally.

Funding

National Science Foundation under the EFRI-PSBR program; Lehigh University Collaborative Research Opportunity (CORE) program.

Notes

The authors declare no competing financial interest.

ACKNOWLEDGMENTS

This material is based upon work supported by the National Science Foundation under the EFRI-PSBR program, Grant No. 1332349. Additional support was received from the Lehigh University Collaborative Research Opportunity (CORE) program.

REFERENCES

(1) Mann, S. Biomineralization: principles and concepts in bioinorganic materials chemistry; Oxford University Press: New York, 2001; Vol. 5.

(2) Nudelman, F.; Sommerdijk, N. A. Biomineralization as an inspiration for materials chemistry. Angew. Chem., Int. Ed. 2012, 51, 6582−6596.

(3) Flynn, C. E.; Lee, S.; Peelle, B. R.; Belcher, A. M. Viruses as vehicles for growth, organization and assembly of materials. Acta Mater. 2003, 51, 5867−5880.

(4) Zhou, J.; Yang, Y.; Zhang, C. Toward Biocompatible Semi-conductor Quantum Dots: From Biosynthesis and Bioconjugation to Biomedical Application. Chem. Rev. 2015, 115, 11669−11717.

(5) Falini, G.; Albeck, S.; Weiner, S.; Addadi, L. Control of aragonite or calcite polymorphism by mollusk shell macromolecules. Science 1996, 271, 67.

(6) Politi, Y.; Arad, T.; Klein, E.; Weiner, S.; Addadi, L. Sea urchin spine calcite forms via a transient amorphous calcium carbonate phase. Science 2004, 306, 1161−1164.

(7) Belcher, A. M.; Wu, X.; Christensen, R.; Hansma, P.; Stucky, G.; Morse, D. Control of crystal phase switching and orientation by soluble mollusc-shell proteins. Nature 1996, 381, 56−58.

(8) Zaremba, C. M.; Belcher, A. M.; Fritz, M.; Li, Y.; Mann, S.; Hansma, P. K.; Morse, D. E.; Speck, J. S.; Stucky, G. D. Critical transitions in the biofabrication of abalone shells and flat pearls. Chem. Mater. 1996, 8, 679−690.

(9) Cha, J. N.; Shimizu, K.; Zhou, Y.; Christiansen, S. C.; Chmelka, B. F.; Stucky, G. D.; Morse, D. E. Silicatein filaments and subunits from a marine sponge direct the polymerization of silica and silicones in vitro. Proc. Natl. Acad. Sci. U. S. A. 1999, 96, 361−365.

(10) Krasko, A.; Lorenz, B.; Batel, R.; Schröder, H. C.; Müller, I. M.; Müller, W. E. Expression of silicatein and collagen genes in the marine sponge Suberites domuncula is controlled by silicate and myotrophin. Eur. J. Biochem. 2000, 267, 4878−4887.

(11) Shimizu, K.; Cha, J.; Stucky, G. D.; Morse, D. E. Silicatein alpha: cathepsin L-like protein in sponge biosilica. Proc. Natl. Acad. Sci. U. S. A. 1998, 95, 6234−6238.

(12) Kröger, N.; Deutzmann, R.; Sumper, M. Polycationic peptides from diatom biosilica that direct silica nanosphere formation. Science 1999, 286, 1129−1132.
(13) Kröger, N.; Deutzmann, R.; Bergsdorf, C.; Sumper, M. Species-specific polyamines from diatoms control silica morphology. Proc. Natl. Acad. Sci. U. S. A. 2000, 97, 14133−14138.
(14) Bourzac, K. Quantum dots go on display. Nature 2013, 493, 7432.
(15) Sanderson, K. Quantum dots go large. Nature 2009, 459, 760.
(16) Alivisatos, A. P.; Gu, W.; Larabell, C. Quantum dots as cellular probes. Annu. Rev. Biomed. Eng. 2005, 7, 55−76.
(17) Nozik, A. Quantum dot solar cells. Phys. E 2002, 14, 115−120.
(18) Zhou, J.; Yang, Y.; Zhang, C. Toward biocompatible semiconductor quantum dots: From biosynthesis and bioconjugation to biomedical application. Chem. Rev. 2015, 115, 11669.
(19) Bera, D.; Qian, L.; Tseng, T.; Holloway, P. H. Quantum Dots and Their Multimodal Applications: A Review. Materials 2010, 3, 2260−2345.
(20) Borovaya, M. N.; Naumenko, A. P.; Matvieieva, N. A.; Blume, Y. B.; Yemets, A. I. Biosynthesis of luminescent CdS quantum dots using plant hairy root culture. Nanoscale Res. Lett. 2014, 9, 1−7.
(21) Kang, S. H.; Bozhilov, K. N.; Myung, N. V.; Mulchandani, A.; Chen, W. Microbial synthesis of CdS nanocrystals in genetically engineered E.coli. Angew. Chem., Int. Ed. 2008, 47, 5186−5189.
(22) Sweeney, R. Y.; Mao, C.; Gao, X.; Burt, J. L.; Belcher, A. M.; Georgiou, G.; Iverson, B. L. Bacterial Biosynthesis of Cadmium Sulfide Nanocrystals. Chem. Biol. 2004, 11, 1553−1559.
(23) Spoerke, E. D.; Voigt, J. A. Influence of engineered peptides cadmium sulfide nanocrystals. Adv. Funct. Mater. 2007, 17, 2031− 2037.
(24) Mao, C.; Flynn, C. E.; Hayhurst, A.; Sweeney, R.; Qi, J.; Georgiou, G.; Iverson, B.; Belcher, A. M. Viral assembly of oriented quantum dot nanowires. Proc. Natl. Acad. Sci. U. S. A. 2003, 100, 6946−6951.
(25) Flynn, C. E.; Mao, C.; Hayhurst, A.; Williams, J. L.; Georgiou, G.; Iverson, B.; Belcher, A. M. Synthesis and organization of nanoscale II−VI semiconductor materials using evolved peptide specificity and viral capsid assembly. J. Mater. Chem. 2003, 13, 2414−2421.
(26) Dameron, C. T.; Reese, R. N.; Mehra, R. K.; Kortan, A. R.; Carroll, P. J.; Steigerwald, M. L.; Brus, L. E.; Winge, D. R. Biosynthesis of cadmium sulphide quantum semiconductor crystallites. Nature 1989, 338, 596−597.
(27) Chen, G.; Yi, B.; Zeng, G.; Niu, Q.; Yan, M.; Chen, A.; Du, J.; Huang, J.; Zhang, Q. Facile green extracellular biosynthesis of CdS quantum dots by white rot fungus Phanerochaete chrysosporium. Colloids Surf., B 2014, 117, 199−205.
(28) Gallardo, C.; Monrás, J.; Plaza, D.; Collao, B.; Saona, L.; Durán-Toro, V.; Venegas, F.; Soto, C.; Ulloa, G.; Vasquez, C. Low-temperature biosynthesis of fluorescent semiconductor nanoparticles (CdS) by oxidative stress resistant Antarctic bacteria. J. Biotechnol. 2014, 187, 108−115.
(29) Bai, H. J.; Zhang, Z. M.; Guo, Y.; Yang, G. E. Biosynthesis of cadmium sulfide nanoparticles by photosynthetic bacteria Rhodopseudomonas palustris. Colloids Surf., B 2009, 70, 142−146.
(30) Cunningham, D. P.; Lundie, L. L., Jr Precipitation of cadmium by Clostridium thermoaceticum. Appl. Environ. Microbiol. 1993, 59, 7− 14.
(31) Yang, Z.; Lu, L.; Berard, V. F.; He, Q.; Kiely, C. J.; Berger, B. W.; McIntosh, S. Biomanufacturing of CdS quantum dots. Green Chem. 2015, 17, 3775−3782.
(32) Dunleavy, R.; Lu, L.; Kiely, C. J.; McIntosh, S.; Berger, B. W. Single-enzyme biomineralization of cadmium sulfide nanocrystals with controlled optical properties. Proc. Natl. Acad. Sci. U. S. A. 2016, 113, 5275−5280.
(33) Spangler, L. C.; Lu, L.; Kiely, C. J.; Berger, B. W.; McIntosh, S. Biomineralization of PbS and PbS−CdS core−shell nanocrystals and their application in quantum dot sensitized solar cells. J. Mater. Chem. A 2016, 4, 6107−6115.
(34) Koneswaran, M.; Narayanaswamy, R. L-Cysteine-capped ZnS quantum dots based fluorescence sensor for Cu(II) ion. Sens. Actuators, B 2009, 139, 104−109.
(35) Liu, W.; Choi, H. S.; Zimmer, J. P.; Tanaka, E.; Frangioni, J. V.; Bawendi, M. Compact cysteine-coated CdSe (ZnCdS) quantum dots for in vivo applications. J. Am. Chem. Soc. 2007, 129, 14530−14531.
(36) Cai, Z.; Yang, H.; Zhang, Y.; Yan, X. Preparation, characterization and evaluation of water-soluble L-cysteine-capped-CdS nanoparticles as fluorescence probe for detection of Hg (II) in aqueous solution. Anal. Chim. Acta 2006, 559, 234−239.
(37) Zhang, Y.; Zhang, H.; Guo, X.; Wang, H. L-Cysteine-coated CdSe/CdS core-shell quantum dots as selective fluorescence probe for copper (II) determination. Microchem. J. 2008, 89, 142−147.
(38) Chen, Y.; Rosenzweig, Z. Luminescent CdS quantum dots as selective ion probes. Anal. Chem. 2002, 74, 5132−5138.
(39) Chatterjee, A.; Priyam, A.; Das, S. K.; Saha, A. Size tunable synthesis of cysteine-capped CdS nanoparticles by γ-irradiation. J. Colloid Interface Sci. 2006, 294, 334−342.
(40) Wang, C.; Lum, A.; Ozuna, S.; Clark, D.; Keasling, J. Aerobic sulfide production and cadmium precipitation by Escherichia coli expressing the Treponema denticola cysteine desulfhydrase gene. Appl. Microbiol. Biotechnol. 2001, 56, 425−430.
(41) Ellman, G. L. Tissue sulfhydryl groups. Arch. Biochem. Biophys. 1959, 82, 70−77.
(42) Chen, D.; Zhao, F.; Qi, H.; Rutherford, M.; Peng, X. Bright and stable purple/blue emitting CdS/ZnS core/shell nanocrystals grown by thermal cycling using a single-source precursor. Chem. Mater. 2010, 22, 1437−1444.
(43) Lippens, P.; Lannoo, M. Calculation of the band gap for small CdS and ZnS crystallites. Phys. Rev. B: Condens. Matter Mater. Phys. 1989, 39, 10935−10942.
(44) Gladysheva, T.; Liu, J.; Rosen, B. P. His-8 lowers the pKa of the essential Cys-12 residue of the ArsC arsenate reductase of plasmid R773. J. Biol. Chem. 1996, 271, 33256−33260.
(45) Tamang, S.; Beaune, G.; Texier, I.; Reiss, P. Aqueous phase transfer of InP/ZnS nanocrystals conserving fluorescence and high colloidal stability. ACS Nano 2011, 5, 9392−9402.
(46) Hu, L.; Zhang, C.; Zeng, G.; Chen, G.; Wan, J.; Guo, Z.; Wu, H.; Yu, Z.; Zhou, Y.; Liu, J. Metal-based quantum dots: synthesis, surface modification, transport and fate in aquatic environments and toxicity to microorganisms. RSC Adv. 2016, 6, 78595−78610.
(47) Nguyen, L.; Kho, R.; Bae, W.; Mehra, R. K. Glutathione as a matrix for the synthesis of CdS nanocrystallites. Chemosphere 1999, 38, 155−173.
(48) Wang, Y.; Hu, R.; Lin, G.; Law, W.; Yong, K. Optimizing the aqueous phase synthesis of CdTe quantum dots using mixed-ligands system and their applications for imaging of live cancer cells and tumors in vivo. RSC Adv. 2013, 3, 8899−8908.
(49) Kimura, H. Hydrogen sulfide: its production, release and functions. Amino Acids 2011, 41, 113−121.
(50) Brown, F. C.; Gordon, P. Cystathionine synthase from rat liver: partial purification and properties. Can. J. Biochem. 1971, 49, 484−491.
(51) Nakagawa, H.; Kimura, H. Purification and properties of cystathionine synthetase from rat liver: separation of cystathionine synthetase from serine dehydratase. Biochem. Biophys. Res. Commun. 1968, 32, 208−214.
(52) Steegborn, C.; Clausen, T.; Sondermann, P.; Jacob, U.; Worbs, M.; Marinkovic, S.; Huber, R.; Wahl, M. C. Kinetics and inhibition of recombinant human cystathionine gamma-lyase. Toward the rational control of transsulfuration. J. Biol. Chem. 1999, 274, 12675−12684.
(53) Priyam, A.; Chatterjee, A.; Das, S.; Saha, A. Synthesis and spectral studies of cysteine-capped CdS nanoparticles. Res. Chem. Intermed. 2005, 31, 691−702.
(54) Gao, M.; Kirstein, S.; Möhwald, H.; Rogach, A. L.; Kornowski, A.; Eychmüller, A.; Weller, H. Strongly photoluminescent CdTe nanocrystals by proper surface modification. J. Phys. Chem. B 1998, 102, 8360−8363.

(55) Li, H.; Shih, W. Y.; Shih, W. Synthesis and characterization of aqueous carboxyl-capped CdS quantum dots for bioapplications. Ind. Eng. Chem. Res. 2007, 46, 2013−2019.
(56) Nosaka, Y.; Yamaguchi, K.; Miyama, H.; Hayashi, H. Preparation of size-controlled CdS colloids in water and their optical properties. Chem. Lett. 1988, 17, 605−608.
(57) Chen, J.; Zheng, A.; Gao, Y.; He, C.; Wu, G.; Chen, Y.; Kai, X.; Zhu, C. Functionalized CdS quantum dots-based luminescence probe for detection of heavy and transition metal ions in aqueous solution. Spectrochim. Acta, Part A 2008, 69, 1044−1052.
(58) Winter, J. O.; Gomez, N.; Gatzert, S.; Schmidt, C. E.; Korgel, B. A. Variation of cadmium sulfide nanoparticle size and photo-luminescence intensity with altered aqueous synthesis conditions. Colloids Surf., A 2005, 254, 147−157.
(59) Negi, D. P.; Chanu, T. I. Surface-modified CdS nanoparticles as a fluorescent probe for the selective detection of cysteine. Nano-technology 2008, 19, 465503.
(60) Chang, C.; Lee, Y. Chemical bath deposition of CdS quantum dots onto mesoscopic TiO2 films for application in quantum-dot-sensitized solar cells. Appl. Phys. Lett. 2007, 91, 053503.
(61) Zhu, G.; Cheng, Z.; Lv, T.; Pan, L.; Zhao, Q.; Sun, Z. Zn-doped nanocrystalline TiO 2 films for CdS quantum dot sensitized solar cells. Nanoscale 2010, 2, 1229−1232.
(62) Zhu, G.; Pan, L.; Sun, H.; Liu, X.; Lv, T.; Lu, T.; Yang, J.; Sun, Z. Electrophoretic Deposition of a Reduced Graphene−Au Nano-particle Composite Film as Counter Electrode for CdS Quantum Dot-Sensitized Solar Cells. ChemPhysChem 2012, 13, 769−773.
(63) Protiere, M.; Reiss, P. Facile synthesis of monodisperse ZnS capped CdS nanocrystals exhibiting efficient blue emission. Nanoscale Res. Lett. 2006, 1, 62−67.
(64) Huang, L.; Wang, X.; Yang, J.; Liu, G.; Han, J.; Li, C. Dual cocatalysts loaded type I CdS/ZnS core/shell nanocrystals as effective and stable photocatalysts for H_2 evolution. J. Phys. Chem. C 2013, 117, 11584−11591.
(65) Steckel, J. S.; Zimmer, J. P.; Coe-Sullivan, S.; Stott, N. E.; Bulović, V.; Bawendi, M. G. Blue luminescence from (CdS) ZnS core−shell nanocrystals. Angew. Chem., Int. Ed. 2004, 43, 2154−2158.